Chapter 6

Mesoscale Convective Systems and Early Development of Tropical Cyclones

Kevin K. W. Cheung and Guoping Zhang

Additional information is available at the end of the chapter

http://dx.doi.org/10.5772/64185

Abstract

This chapter studies two Tropical cyclone (TC) cases, Typhoon Dan (1999) and Typhoon Ketsana (2003), and discusses their rates of formation and relationship with the mesoscale convective activities through examining the numerical simulations of the two cases. Many TCs generate from a single mesoscale convective System (MCS) or multiple MCSs; the physical processes under these two patterns are found to include dissipation of convection leading to new eruptions of deep convection located near the edge of the dissipating convection core, ingestion of nearby convection, merging of multiple MCSs into one MCS, and merging of deep convection within the MCS associated with the aggregation of vorticity in early development stage of TCs. How these activities lead to the formation of Typhoon Ketsana has been diagnosed. The diabatic heating associated with these convective activities also help to form the TC warm core. The relationship between the rate of TC formation and early development and convection energy consumption is discussed.

Keywords: tropical cyclone formation, mesoscale convective systems, stratiform and convective rain, diabatic heating, convective available potential energy

1. Introduction

Over the recent decades, researches for the process that generates a surface vortex have focused on the observation that TC formation is associated with mesoscale convective systems (MCSs) and their accompanying mesoscale convective vortices (MCVs). It was believed that the transition from MCS to a TC-like vortex required the generation of low-level cyclonic vorticity below the MCS, and researches for TC genesis mechanisms focus on what provided this sub-MCS low-level cyclonic vorticity. It is common to observe MCS or MCSs involved in

the formation process of TCs in the western North Pacific (WNP). Over 63% of the studied TCs have multiple MCS convection appearing at the formation process, and 35% have the single MCS appearing at the beginning of the formation process. About 90% of cases with a shorter time period of formation process (within 6 h) have single MCS [1]. The physical processes under the single MCS and multiple MCS convection are found to include dissipation of convection leading to new eruptions of deep convection located near the edge of the dissipating convection core, ingestion of nearby convection, merging of multi-MCSs into single MCS, and merging of deep convection within the MCS associated with the aggregation of vorticity in fast formation process.

An MCS is organized as convective cloud clusters, and TC formation process is due to increasing organizition of MCS, which is caused by accumulation of mesoscale vorticity [2]. Convective activities resulted from thermodynamic and/or dynamic effects that affect the evolution of early development of TCs [3, 4]. They play critical roles in the formation process on TCs; furthermore, the local warming and diabatic heating associated with these convective activities also help to spin up the circulation and generate the warm core structure. How the pattern of MCS convection affects the rate of TC formation and early development is the focus of this chapter. In this chapter, two TC cases are studied and their synopses are first provided before their rates of development are discussed. The model simulations of the two cases are validated in terms of synoptic development and convective episodes. The convection types in the model are separated into convective and stratiform types with their respective vertical heating profiles. Then the heating associated with the MCSs and its effect on TC development are analyzed based on previous theories [5] and through Eliassen–Palm (EP) flux analysis. Then, the rates of development in the two TC cases are discussed based on the convective energy consumption point of view. In regard to this view, convection development and maintenance consume convective available potential energy (CAPE) in their local environment. It gradually makes the local environment less conducive for further convection development, which may affect the temporal evolution of TC formation when the surface vorticity is still below the threshold for tropical storm. However, it humidifies the middle and upper troposphere, and then gradually builds up the value of CAPE again in the local environment until new deep convection bursts up.

2. Typhoon cases and numerical simulations

The numerical experiments in this study include two case studies: Typhoon (TY) Ketsana (2003) with the development of multiple MCSs and Typhoon Dan (1999) with only one MCS involved during its formation. These experiments are then examined to study the difference in the formation time and energy consumption in the two cases. In the simulations for both typhoon cases, the same set of nested domain settings is applied, and the same satellite datasets have been assimilated via the Weather Research and Forecasting Data Assimilation (WRFDA) system.

http://dx.doi.org/10.5772/64185

In the WRF simulation of Typhoon Ketsana, the model's initial and lateral conditions are taken from the National Center for Environmental Prediction (NCEP) final (FNL) analysis data with the outermost lateral boundary conditions updated every 6 h, and the SST data are interpolated to update the sea-surface boundary conditions. The WRF model is initialized at 0000 UTC on October 16, 2003 and integrated for 108 h until 1200 UTC on October 20. Within this model integration period, the WRFDA is used to assimilate QuikSCAT oceanic winds available at 0600 UTC on October 16 and 0600 UTC on October 17, 2003, and SSM/I oceanic surface wind speed and total precipitable water (TPW) available at 1200 UTC on October 17, 2003 into the boundary conditions. These twice daily swaths of QuikSCAT and SSM/I data are extracted from the remote sensing system (RSS) data archive with 0.25° latitude/longitude resolution.

The WRF simulation of Typhoon Dan (1999) is initialized at 0000 UTC on October 1, 1999 and integrated for 120 h until 0000 UTC on October 6. Similar to the case of Typhoon Ketsana, the WRFDA is used to assimilate QuikSCAT oceanic winds available at 0600 UTC on October 1 and 0600 UTC on October 2, and SSM/I oceanic surface wind speed and TPW available at 1200 UTC on October 1 and 12 UTC on October 2 into the boundary conditions.

3. Synopses of Typhoon cases

3.1. Synopsis of Typhoon Ketsana (2003)

In the middle of October 2003, Typhoon Ketsana initially developed from a disturbance embedded in a reversed-oriented monsoon trough between Luzon and Guam (about 1296 km east of Luzon Island) on October 15, 2003 (**Figure 1**). The monsoon trough provided a favorable large-scale environment with high humidity and abundant low-level cyclonic vorticity for TC formation. For several days, the system remained disorganized while drifting to the west–northwest due to weak steering currents, south of the subtropical ridge. The disturbance developed into a tropical depression at 1200 UTC on October 18 (taken as formation time), and on October 19, the Japan Meteorological Agency (JMA) upgraded the depression to tropical storm, and by that time the storm had begun drifting to the northeast. Throughout the days of October 20-21, movement was slow with only weak northeasterly steering currents controlling Typhoon Ketsana, although the intensification was not so slow. With favorable outflow, Ketsana quickly intensified and was upgraded into a typhoon at 1200 UTC on October 20. After an eye formed, the slow motion continued throughout the day as did intensification. By 1200 UTC on October 21, the intensity had reached the lifetime peak intensity of 125 kt. Ketsana started weakening at 1800 UTC on October 22, with the intensity falling to 115 kt.

At 0000 UTC on October 23, Typhoon Ketsana moved slowly northeastward, but a weakening trend had set in and began to accelerate the next day, with evidence of a mass of stratocumulus cloud to the northwest of Ketsana, showing the presence of colder, drier, and more stable air. At 0000 UTC on October 24, Ketsana was beginning extratropical transition. Drier air had

penetrated into the circulation and went northeastward into the westerlies with doubled forward speed.

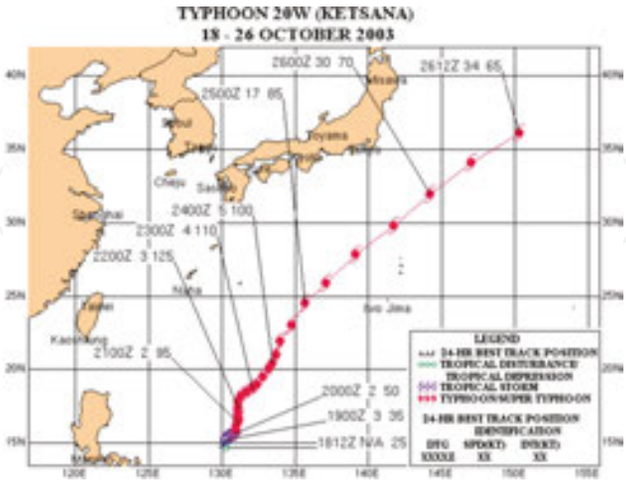

Figure 1. Best track of Typhoon Ketsana (2003) from the JTWC (adapted from Ref. [6]).

3.2. Synopsis of Typhoon Dan (1999)

Typhoon Dan (1999) first developed over the Philippine Sea at 1200 UTC on October 1, 1999 to the east of Island Luzon. The Joint Typhoon Warning Center (JTWC) issued a TC formation alert at 0230 UTC on October 2. When deep convection was seen to build over the low-level circulation center from the south near 1500 UTC on October 2, the first warning of the TC was issued by the JTWC. The system further developed into a tropical depression about 1140 km east–northeast of Manila on October 3 (taken as formation time at 1200 UTC on October 3, 1999) and then moved westward (**Figure 2**). Dan intensified very fast to a tropical storm and

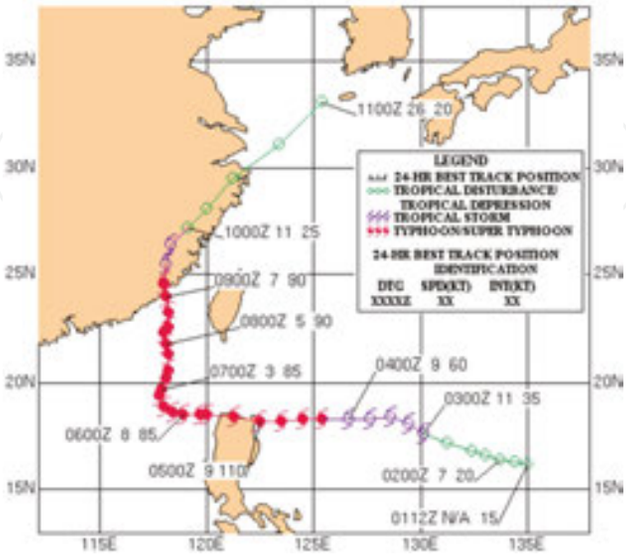

Figure 2. Best track of Typhoon Dan (1999) from the JTWC (adapted from Ref. [7]).

http://dx.doi.org/10.5772/64185

then a typhoon the next day. It reached a peak intensity of 110 kt (56.9 m/s) when affecting the Northern Luzon coast on October 5. TY Dan then moved over the South China Sea and weakened when it entered an increased vertical wind shear environment. It slowed down the next day and abruptly turned northward on October 7 with slight re-intensification. It eventually made a landfall near Xiamen, Fujian, China on October 9 and then weakened overland. Dan turned to the northeast and weakened to a tropical depression before it moved over the Yellow Sea later on October 10.

4. MCSs analysis

One of the characteristics of TC formation in the monsoon trough is frequent development of MCSs due to low-level convergence that enhances convection. The definition of MCS in Ref. [8] (i.e., area >1000 km^2 within the brightness isotherm −52°C) is applied. During the 48 h (1200 UTC, October 16–18) prior to Typhoon Ketsana's formation, five MCSs are observed. The first two developed on October 16 and early October 17, respectively. Later, MCS3 and MCS4 developed almost simultaneously near 1500 UTC on October 17, but then dissipated (**Figure 3**). The fifth MCS5 developed at 0600 UTC on October 18 near the low-level circulation center, and led to the formation of the typhoon 6 h later.

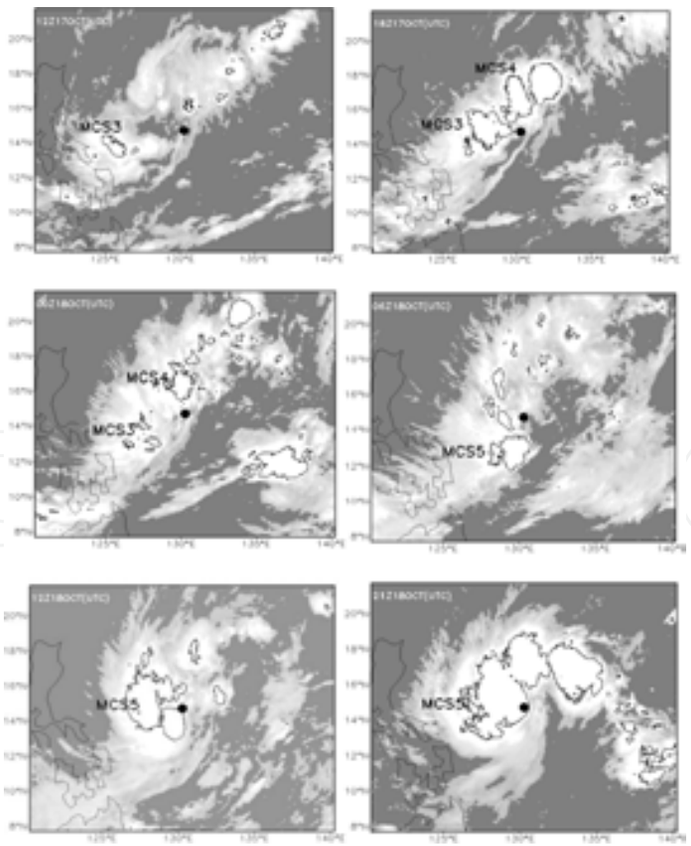

Figure 3. Six-hourly IR1 satellite images from 1200 UTC on October 17, 2003 to 1800 UTC on October 18, 2003. The contour is TB of −75°C, and the black dot is the best-track location of Ketsana's formation (adapted from Ref. [10]).

Figure 4 shows the development process of the formation of Typhoon Dan. Since October 1, 1999, there were many weak tropical convective clusters formed and maintained. At 1200 UTC on October 2, one of the cloud clusters started to develop and kept expanding to form a MCS at 0000 UTC on October 3 and then further developed to a tropical depression at 1200 UTC the same day. In contrast to Typhoon Ketsana, there was only one MCS that appeared during the formation process of Dan. While Lee et al. [1] identified that many of the TC cases with single MCS during formation were associated with easterly wave, filtered low-level winds (based on a simple running mean technique with similar low-pass effect of 3–8 days as in Ref. [9]) do not reveal wave activity during the formation of Typhoon Dan. Thus, Typhoon Dan is also classified as a typical monsoon trough formation. The focus here is the single MCS configuration associated with Typhoon Dan's formation in contrast to that of Typhoon Ketsana, with both cases embedded in similar environmental setting.

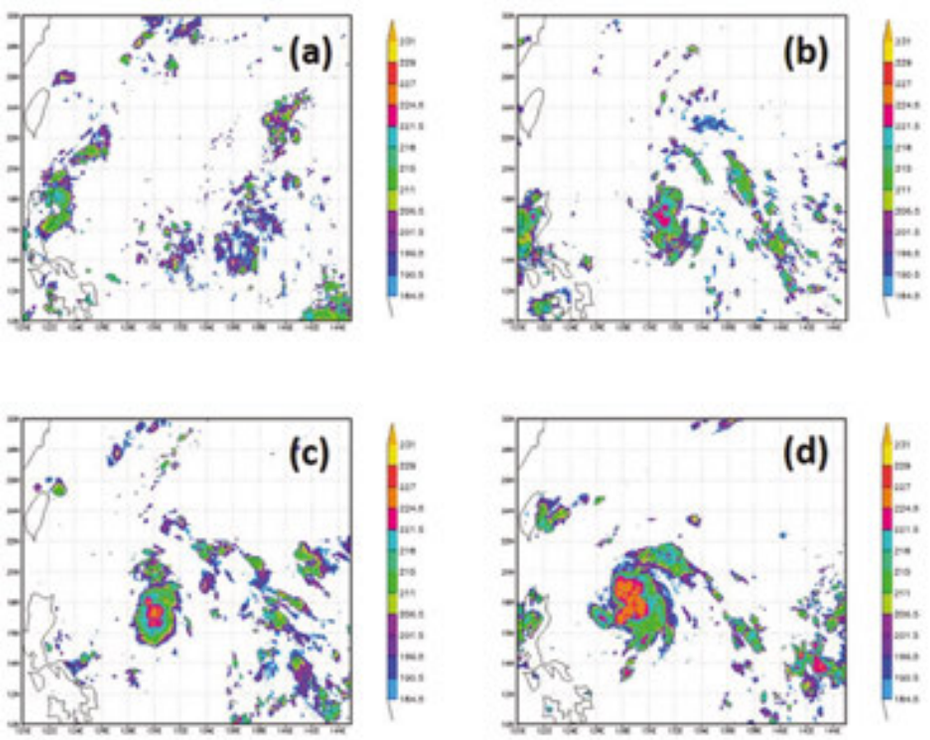

Figure 4. MCSs involved in the formation process of Typhoon Dan at (a) 0500 UTC on October 1, (b) 1200 UTC on October 2, (c) 0000 UTC on October 3, and (d) 1200 UTC on October 3, 1999. Raw pixel values have been shown. (Source: JMA GMS-5 infrared channel-1 data).

5. Model validation for Typhoon Dan

5.1. Synoptic flow

When comparing the NCEP FNL operational analysis data with the WRF simulation of Typhoon Dan in the large domain, it can be seen that the large-scale circulation has been

http://dx.doi.org/10.5772/64185

simulated well. In the FNL analysis, there are two cyclonic regions at about 130°E and 140°E (**Figure 5**). The WRF model mainly developed the incipient vortex circulation at 130°E that eventually became Typhoon Dan. Such consistency with the analysis at the low and mid (not shown) levels provides the conditions for the right timing of TC formation in the model. At the upper level, the simulated subtropical high is located north of where Typhoon Dan is developing, with the maximum high pressure center east of the Taiwan island. This is well verified by the FNL analysis (**Figure 6**), and the system provides good outflow for the formation of Typhoon Dan during its development. The simulated formation position (based on identified near-surface circulation center) and early westward motion of Typhoon Dan match with the best track very well (**Figure 7**), with the formation only a small distance east of the actual position.

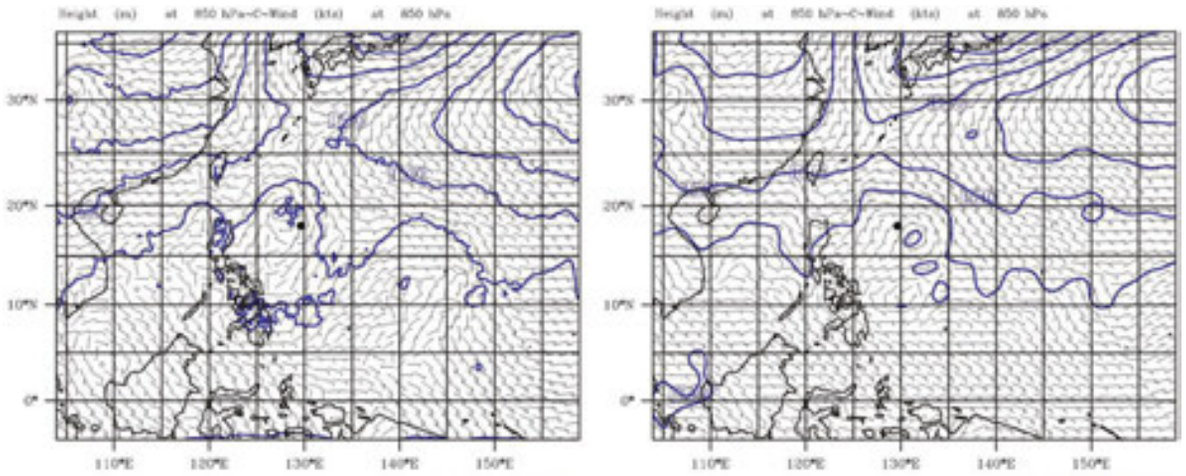

Figure 5. Simulated (left) and FNL analyses (right) of 850 hPa geopotential height (m) and wind barbs at 2000 UTC on October 3, 1999.

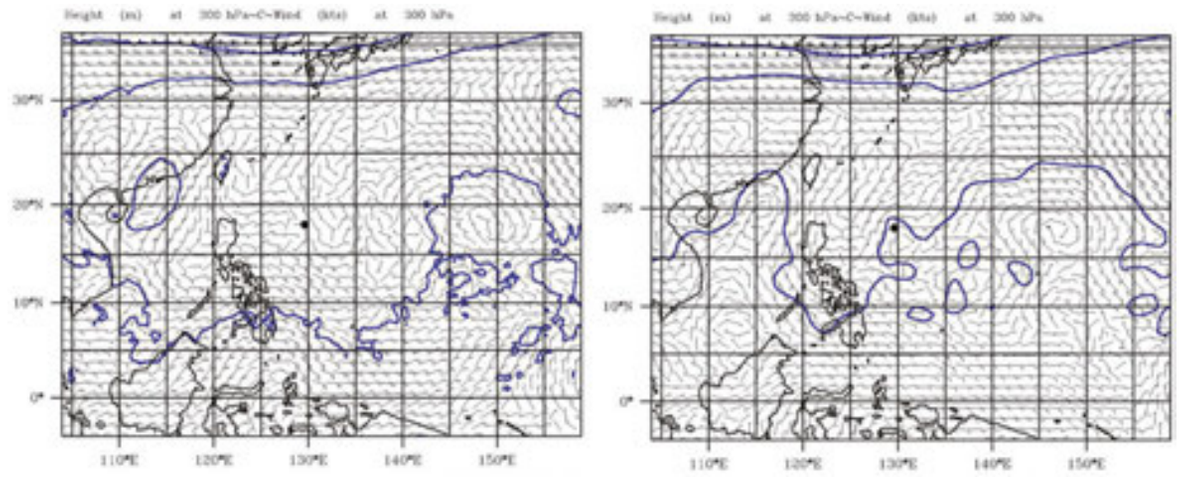

Figure 6. Simulated (left) and FNL analyses (right) of 300 hPa geopotential height (m) and wind barbs at 2000 UTC on October 3, 1999.

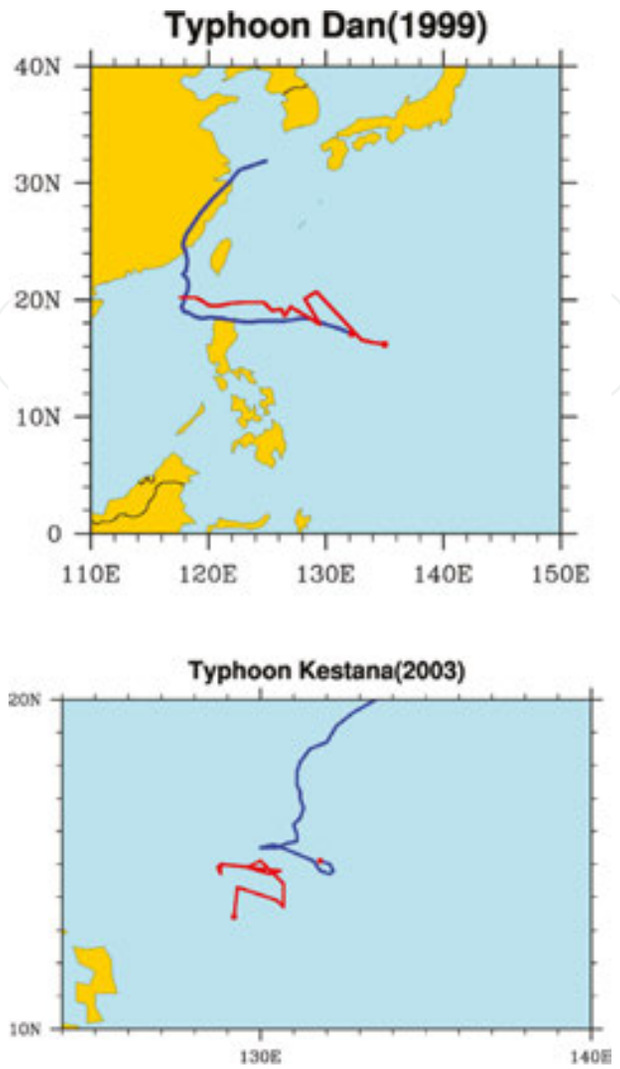

Figure 7. Simulated (red) and JMA best track (blue) of Typhoon Dan (upper) and Ketsana (lower) during 0000 UTC, October 3–6, 1999 and 1200 UTC, October 17–20, 2003 (best track has been extended after October 20, 2003 for Ketsana).

The model validation for Typhoon Ketsana has been presented in detail in Ref. [10], and thus not repeated here. The WRF model applied here is the same version as that used in Ref. [10]. The simulation of Typhoon Ketsana in this study well reproduced the reversed oriented monsoon trough in October 2003 as well as the convection episodes of all MCSs associated with Typhoon Ketsana's formation. The simulated formation position of Ketsana is southwest of the best-track position (**Figure 7**); however, the weak steering flow during the early development has been well simulated.

5.2. Evolution of MCS and intensity

In Ref. [8], the area-average observed TB from satellite images shows a minimum at around 2100 UTC on October 17, 2003 that is associated with MCS3 and MCS4, and then there is another major decrease before formation associated with MCS5 (**Figure 5b** of Ref. [10]). Simulated radar

http://dx.doi.org/10.5772/64185

reflectivity is used to examine convection activity in the model. The time series of simulated radar reflectivity has a local maximum at the same time of occurrence of MCS3 and MCS4. It then increases rapidly 6 h before Ketsana's formation, which is due to convective bursts within MCS5 and is consistent with the observed variation of the area-average TB. The simulated positions of these MCSs also match with those in satellite images: MCS3 was east of the low-level circulation center, and later MCS5 developed at a similar position (**Figure 8**). In terms of intensity, it can be seen that the simulated storm intensifies at the similar rate as observation before formation, however, becoming too intense in the rest of the simulation (**Figure 9**).

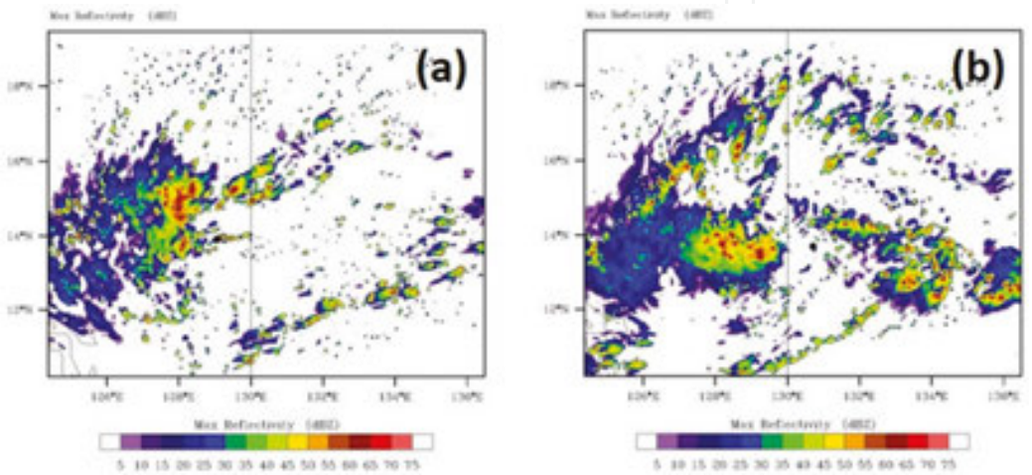

Figure 8. Simulated radar reflectivity (dbZ) of Typhoon Ketsana at (a) 1500 UTC on October 17 and (b) 0600 UTC on October 18, 1999.

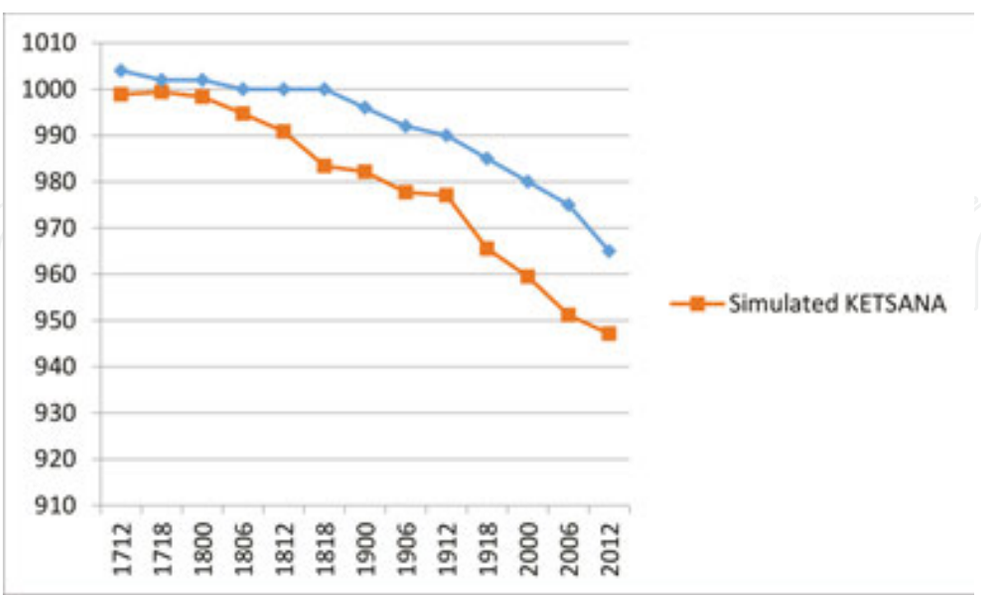

Figure 9. Simulated (red) and JMA best-track minimum surface pressure (hPa) of Typhoon Ketsana during 0000 UTC, October 17–20, 2003.

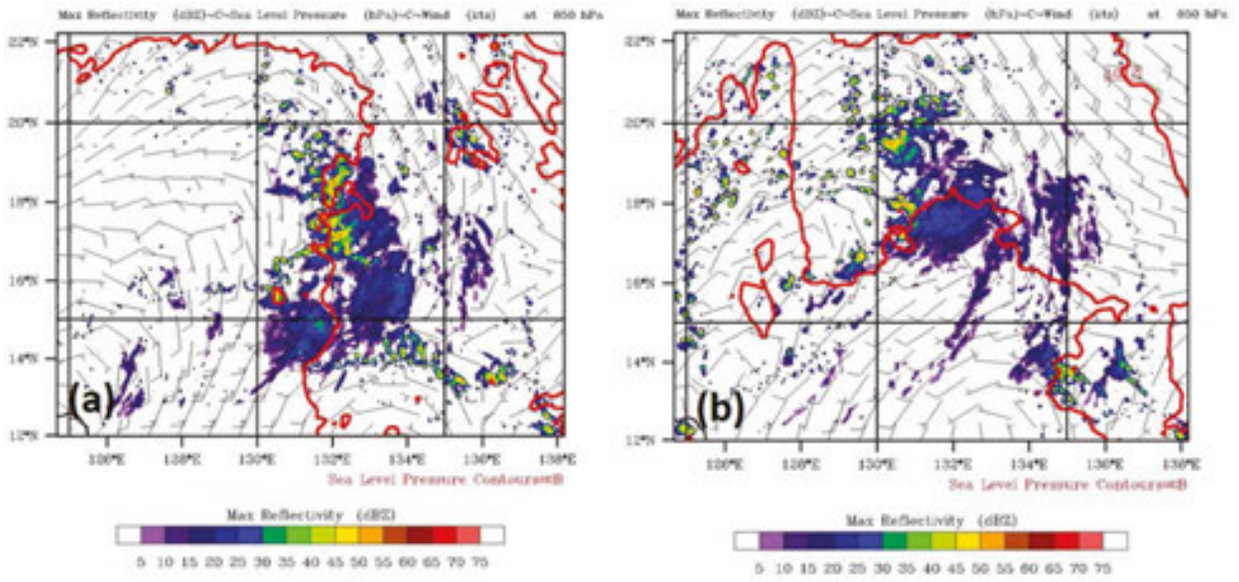

Figure 10. Simulated mean sea-level pressure, 850-hPa wind barbs, and maximum radar reflectivity at 0300 UTC on October 2 (a) and 0700 UTC on October 2, 1999 (b).

The simulated MCS activities of Typhoon Dan are also examined via the simulated radar reflectivity. In early October 2, 1999, the model simulated patches of convection on the eastern side of the broad cyclonic circulation within the monsoon trough (**Figure 10**). A few hours later, the convection organized into a MCS northeast of the circulation center. Such convection persisted when the incipient vortex moved northwestward and intensified. At the beginning of formation, there were still some weak convective cloud clusters that developed slowly until the only MCS formed. In the early formation stage, the model has not captured the initial rate of intensification very well. In the simulation, the surface pressure only started to drop from about 0000 UTC on October 3 (**Figure 11**). Nevertheless, the convection pattern that developed from the single MCS has been reproduced well in the model. From October 3, the simulated intensification rate was similar to that in the best track, and by the end of simulation the TC was more intense than that Typhoon Dan actually attained.

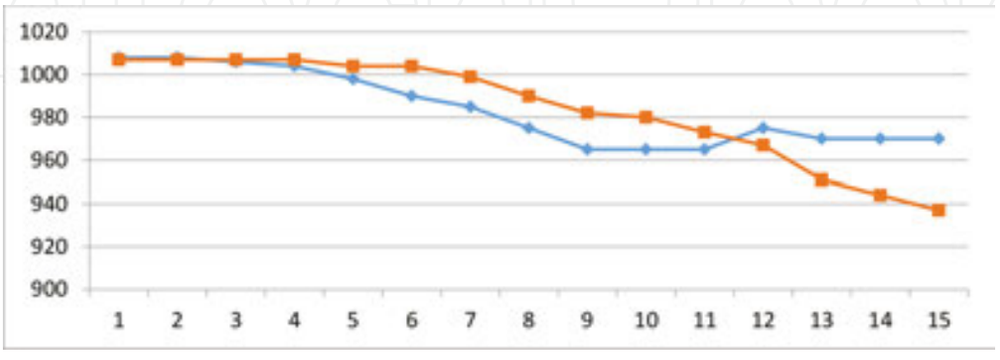

Figure 11. Six-hourly time series of simulated (red) MSLP (hPa) and that in JMA best track (blue) from 1200 UTC on October 2, 1999.

http://dx.doi.org/10.5772/64185

6. Mesoscale heating and early development in Typhoon Ketsana

6.1. Axisymmetric structure

It can be seen from the synopsis and model validation of Typhoon Ketsana that the MCS developments during its formation were highly spatially asymmetric with respect to the low-level circulation center. These MCSs would impose vorticity enhancement and heating effect to the system-scale vortex. Before such responses are analyzed, the axisymmetric structure in the simulation is first examined through the azimuthal mean of tangential and radial wind. The system center is taken as the surface circulation center.

On October 17, the axisymmetric structure of the simulated Typhoon Ketsana shows a broad low-level cyclonic circulation (**Figure 12a**). The maximum tangential wind is below 850 hPa and located between 150 and 200 km from the center. This broad circulation is consistent with the early MCS activities during that day when the first four MCSs developed more than 100 km away from the center. There was only a small region of inflow below 950 hPa, and thus the secondary circulation has not been set up in this stage.

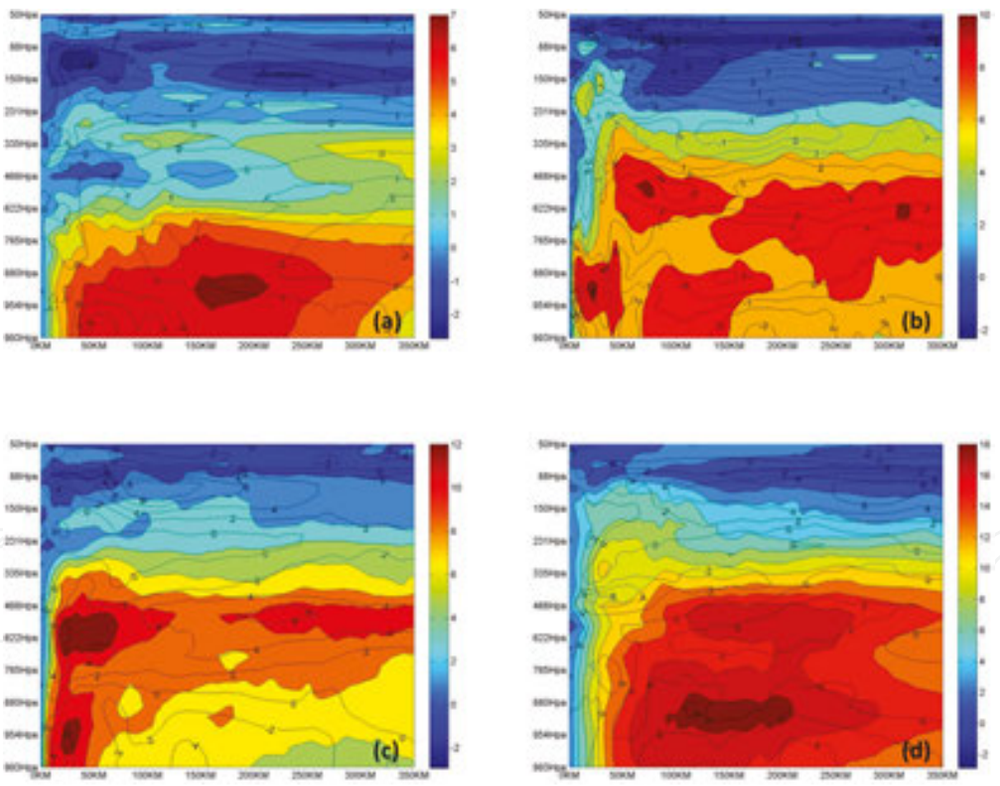

Figure 12. Azimuthal average of tangential (shaded) and radial (contour) wind (m/s) at (a) 1500 UTC on October 17, (b) 0800 UTC on October 18, (c) 1000 UTC on October 18, and (d) 0600 UTC on October 19.

On October 18, when MCS5 developed near the system center, strong low-level tangential winds started to move inward within 50 km, and at the same time extended to the midlevels (**Figure 12b, c**). The eyewall structure has been established just before the formation time of

1200 UTC on October 18. The radial winds also reveal the secondary circulation of inflow below about 800 hPa and outflow above 150 hPa.

Less than a day after the formation time, a mature axisymmetric structure is observed in the simulation. The most intense tangential winds concentrated at about 850 hPa and have been extended from 100 to 200 km from the center (**Figure 12d**). The eyewall structure is clear, and the eye has been enlarged.

6.2. Diabatic heating associated with the MCSs

It is well known that convective-type and stratiform-type rain, besides their respectively unique microphysical nature, are associated with different diabatic heating profiles [11, 12]. The latter is important to the process of vorticity enhancement and warm core during TC development. Convection is associated with deep tropospheric heating, while stratiform rain is associated with upper-level heating but possibly low-level cooling due to evaporation.

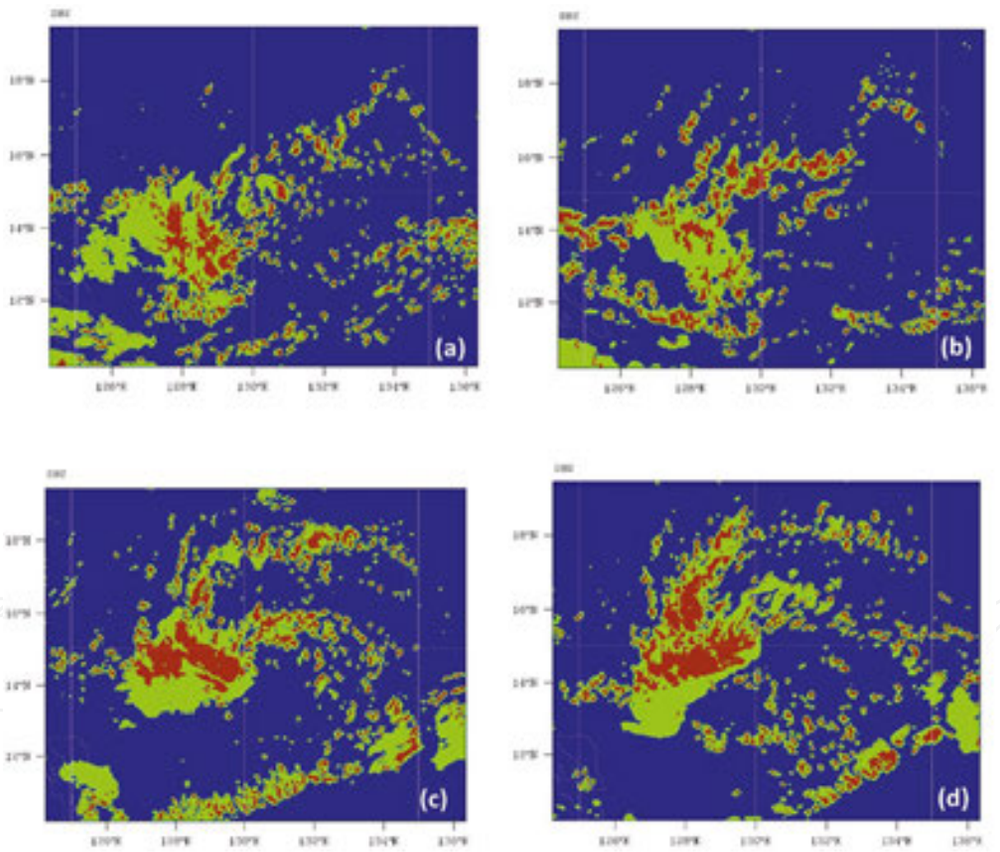

Figure 13. Convective (red) and stratiform (green) rainfall in simulated Typhoon Ketsana at (a) 1200 UTC on October 17, (b) 1500 UTC on October 17, (c) 0800 UTC on October 18, and (d) 1200 UTC on October 18, 2003.

The method in Refs. [13] and [14] is used to separate the two types of rain in Typhoon Ketsana based on the simulated radar reflectivity. The identification of the convective rainfall has further confirmed the MCS activities during the typhoon's development. On October 17, 2003,

http://dx.doi.org/10.5772/64185

among the larger stratiform rain patches, the convective rain concentrated first to the west of the low-level circulation center (which was near 130°E, 14°N), and a few hours later to the north and northeast (**Figure 13a, b**). This is consistent with the temporal evolution of the deep convection from MCS3 to MCS4.

In early October 18, 2003, deep convection occurred again but much closer to the low-level circulation center, which is associated with MCS5. The deep convection persisted until the formation of the cyclone (**Figure 13c, d**). On the other hand, the stratiform rain areas are much larger than the convective areas at all times, which is similar to the partition of other TC cases based on the observed rainfall [15].

When the simulated diabatic heating in WRF is examined, the maximum heating is identified to locate around the midlevel, with extension from about 850 hPa up to 200 hPa. The spatial distribution of maximum heating is confined to specific locations and thus attributed to the deep convection episodes. For example, the azimuthal average of diabatic heating during October 17 shows tropospheric heating positions mostly outside the radius of 50 km, which is likely due to the early MCS activities (**Figure 14a, b**). The maximum heating of these early episodes is of the order of 10^{-3} K/s.

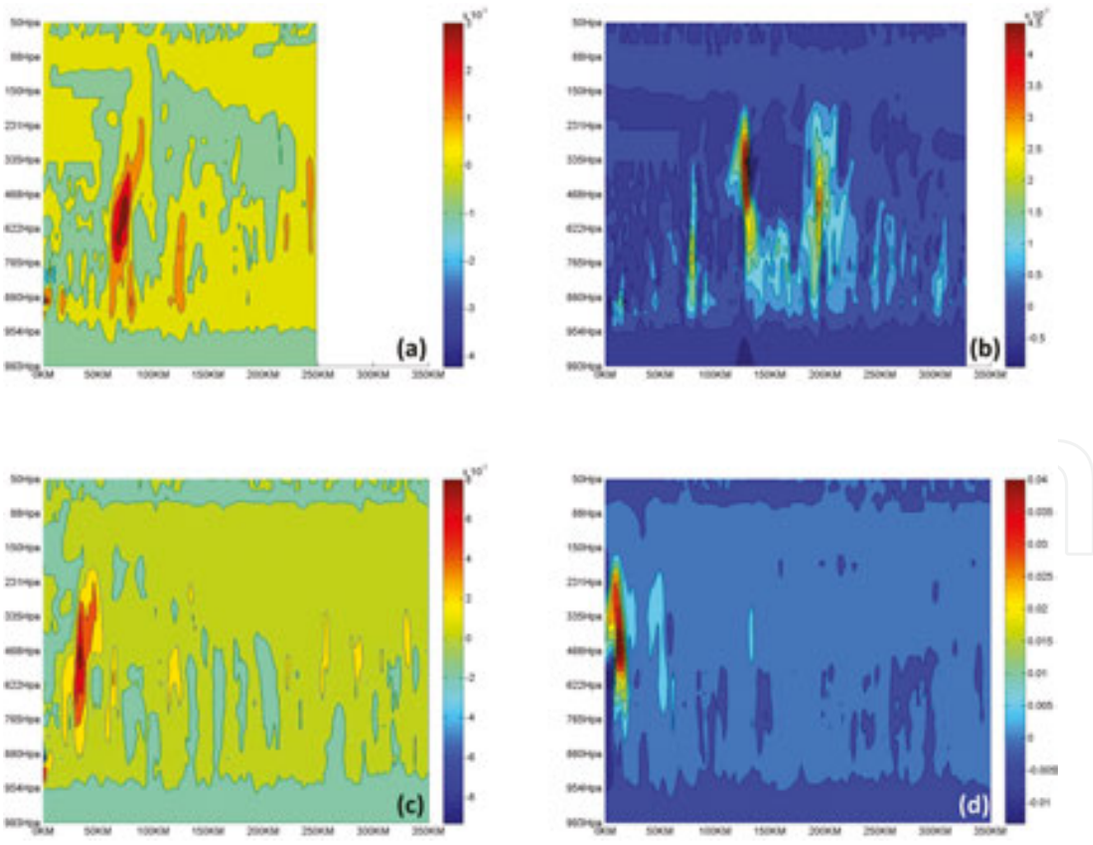

Figure 14. Azimuthal average diabatic heating in simulated Typhoon Ketsana at (a) 1600 UTC on October 17, (b) 2300 UTC on October 17, (c) 0500 UTC on October 18, and (d) 0800 UTC on October 18, 2003. Note the changes in scales.

In early October 18, it can be seen that maximum heating occurs within 50 km that is associated with the last convection episode before the formation of Ketsana (**Figure 14c**). The heating location further moves inward to the circulation center and increases in magnitude about an order higher than the previous episodes (**Figure 14d**).

6.3. Responses to diabatic heating

Reference [5] analyzed the responses of a weak TC vortex to diabatic heating based on the analytical solution of the balanced vortex model, which leads to rapid development toward the steady state with a mature warm-core thermal structure. It was found that the responses depend on the radial location of the diabatic heating. In particular, three factors of static stability, baroclinity, and inertial stability are involved in critical formulating of the responses, especially the inertial stability that usually varies substantially with the radius in a TC vortex. Diabatic heating would be most effective when it is located within the high inertial stability region, which is inside the radius of maximum wind. When the heating position is outside the radius of maximum wind, rapid development is not likely. Thus, based on these theoretical results, the convection episodes associated with the MCSs in the case of Typhoon Ketsana are increasing in heating efficiency for forming the TC. The diabatic heating in the earlier MCSs is outside the inner core with high inertial stability, which is mostly inside radius of 50 km (**Figure 15a**). This is consistent with the simulated TC that shows only slowly intensifying low-level winds in the outer region. During early October 18, when the TC incipient vortex is becoming more intense, the high inertial stability region expands slightly (**Figure 15b**). When the last convection episode associated with MCS5 occurs, the heating sits mostly in that region and is thus able to spin-up the inner-core winds rapidly (**Figure 12c**) and lead to TC formation.

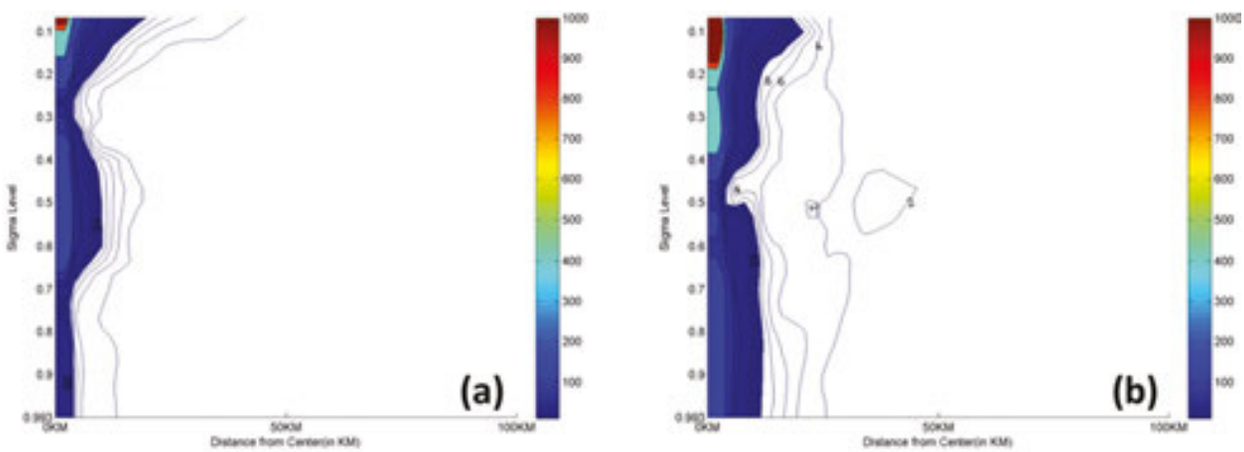

Figure 15. Inertial stability in the simulated Typhoon Ketsana at (a) 0600 UTC on October 17 and (b) 0800 UTC on October 18, 2003, which correspond to **Figure 14a, d**.

Another way to examine the effects of diabatic heating, especially that with azimuthally asymmetric distribution and thus possessing eddy heat flux, is through the EP fluxes [16–20].

http://dx.doi.org/10.5772/64185

The EP fluxes on isentropic coordinates are calculated and analyzed for the simulated Typhoon Ketsana. The EP flux vector consists of the horizontal and vertical components, which correspond to angular momentum flux and heat flux, respectively. The divergence of the flux vector indicates the flux gradients.

During October 17, it can be seen that the EP fluxes with large divergences are mostly scattered at the large radii outside 200 km and concentrated at the lower levels (**Figure 16a**), which are associated with the heating of the earlier MCS convection episodes. The magnitudes of the low to midlevel flux vectors are larger outside 200 km compared with the inner core. The outward directions of these flux vectors indicate inward transport of angular momentum fluxes. There are also small upward components of these flux vectors, indicating inward heat fluxes.

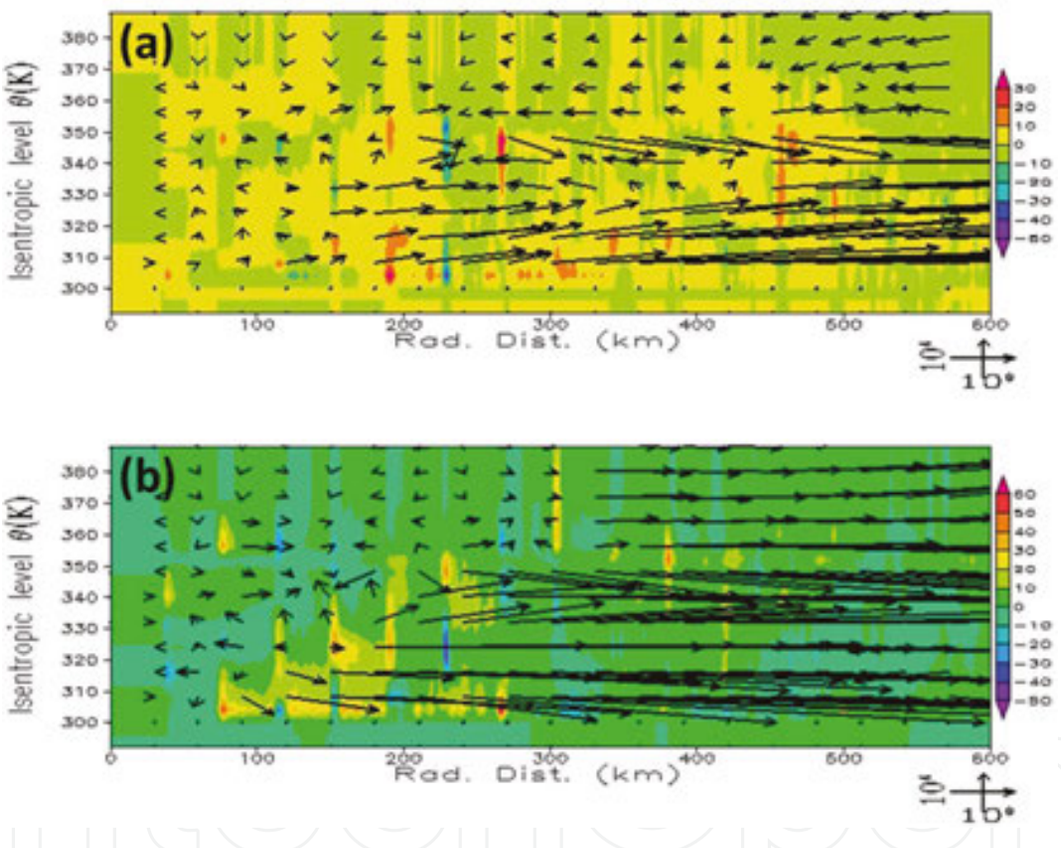

Figure 16. Divergence (contour) of the EP flux vector (arrow) in simulated Typhoon Ketsana at (a) 1200 UTC on October 17 and (b) 1800 UTC on October 18, 2003.

The locations of the largest EP flux divergence remain in the outer region throughout October 17, and then move inward during early October 18. Sometimes, the EP flux vector directions show outward transport of angular momentum in the outer low to midlevel region, which is likely due to spinning up of the outer winds. Right after the formation of the typhoon, the EP flux divergence near the inner core is still strong (**Figure 16b**). Outside radius of 100 km strong magnitudes of outward EP flux vectors indicated inward angular momentum transport again when the core vortex of the typhoon develops rapidly.

7. CAPE and the rate of TC formation

While both typhoons Dan (1999) and Ketsana (2003) formed in similar location of the WNP and the same month of year, their rates of formation were very different. Typhoon Dan developed from a disturbance to tropical depression in about 1 day; however, Typhoon Ketsana took 2 days to form from the initial MCS convection. What factors lead to these different rates of TC development? In this section, this question is examined through the CAPE consumption and recovery point of view.

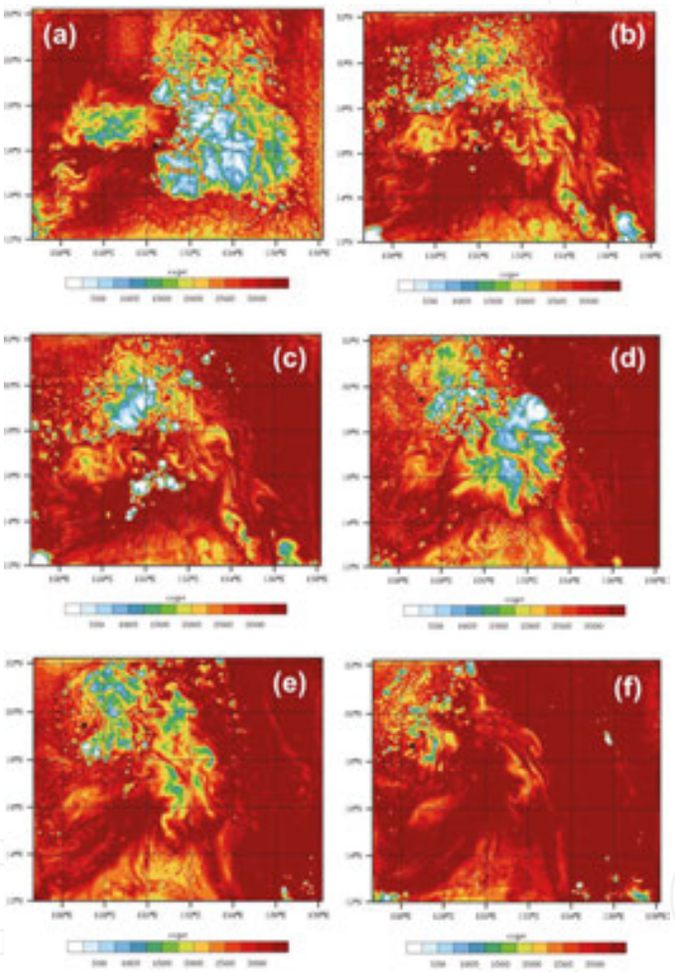

Figure 17. Simulated surface-based CAPE for Typhoon Dan at (a) 0300 UTC on October 2, (b) 1200 UTC on October 2, (c) 1500 UTC on October 2, (d) 0000 UTC on October 3 (e) 0600 UTC on October 3, and (f)1200 UTC on October 3, 1999.

When Typhoon Dan started to develop on October 2, 1999, the CAPE in the region was quite low (**Figure 17a**). The only source of high CAPE was from the southwest of the incipient circulation center. This region of high CAPE persisted throughout the day of October 2, 1999 to support the convection development of the MCS (**Figure 17b**). After the convection further developed near the circulation center, the CAPE was lowered in the region (**Figure 17c**). When the disturbance attained near-tropical low intensity at 0000 UTC on October 3, the low-level

http://dx.doi.org/10.5772/64185

circulation center migrated to the northwest into a region still of quite low CAPE (**Figure 17d**). In other words, throughout the early development of Typhoon Dan, the CAPE with high value in that area was enough to support the development of one MCS, which was close to the low-level circulation center to establish the surface winds effectively. Thus, multiple MCSs development before formation has not been observed in this case. However, the CAPE recovered rapidly after the formation of Typhoon Dan (**Figure 17e, f**), which was good to support further intensification of the storm. This can also be identified in the area-average CAPE in **Figure 18** (the control experiment), which shows the CAPE consumption from 1200 UTC on October 2 to 0000 UTC on October 3, and then the rapid increase thereafter.

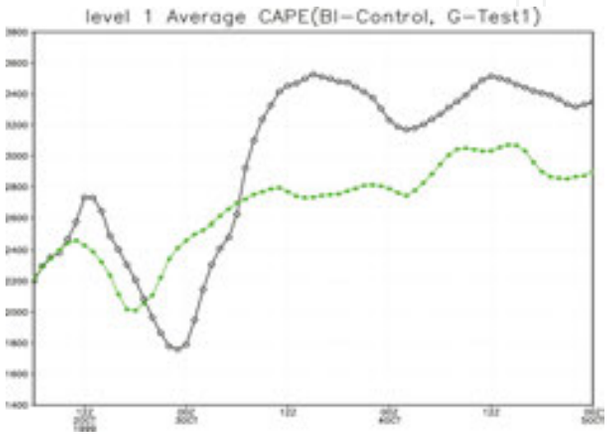

Figure 18. Area-averaged (13–17°N, 127–132°E) surface-based CAPE during formation of Typhoon Dan in the control WRF experiment (black) and sensitivity test (green).

On the other hand, the formation of Typhoon Ketsana (2003) experienced multiple cycles of CAPE consumption and recovery associated with the MCS episodes of convection. After the first two MCSs dissipated in early October 17, the CAPE on the western side of the incipient vortex was clearly lowered (**Figure 19a**). The CAPE did not recover much, and thus the two later MCSs on the same day actually developed out of only moderate values of CAPE. Their consumption of CAPE further lowered the values on the west and north sides of circulation (**Figure 19b**). At about 0600 UTC on October 18, high CAPE values entered the core region of the vortex, which supported the last (fifth) MCS to develop near the center and led to the formation of Typhoon Ketsana at 1200 UTC on October 18 (**Figure 19c, d**). The last MCS dissipated near 0000 UTC on October 19 (**Figure 19e**) that remained with low CAPE values in the core. After that the TC vortex sustained and high CAPE values reappeared associated with the eyewall convection (**Figure 19f**).

Therefore, the development of Typhoon Ketsana during the 2 days before formation was much driven by convection and thus related to the variation of CAPE in the area of development. The convection episodes associated with the MCSs spun up the winds first at the periphery and then in the core, and led to formation of the typhoon, because the four early MCSs formed and developed northwest of the core. This process was quite slow compared with the single MCS development in Typhoon Dan.

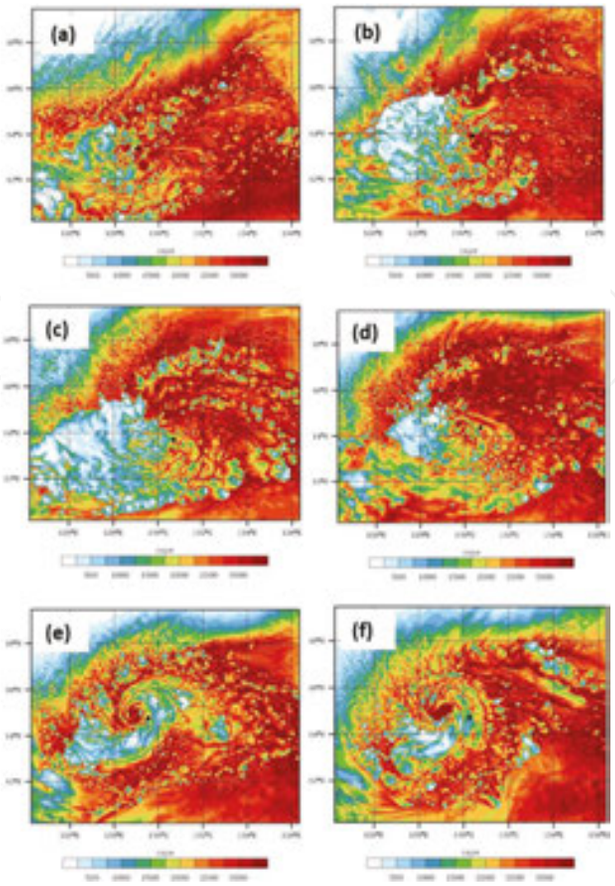

Figure 19. Simulated surface-based CAPE for Typhoon Ketsana at (a) 1200 UTC on October 17, (b) 0000 UTC on October 18, (c) 0600 UTC on October 18, (d) 1200 UTC on October 18, (e) 0000 UTC on October 19, and (f) 0700 UTC on October 19, 2003.

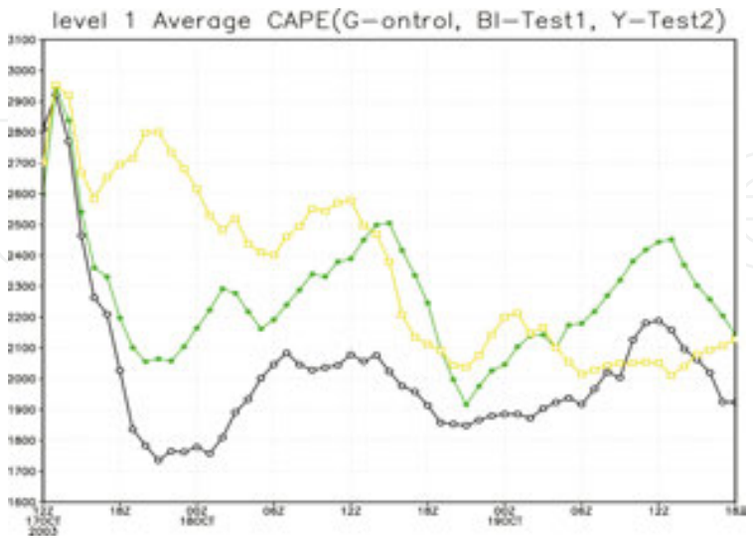

Figure 20. Area-averaged (13–17°N, 127–132°E) surface-based CAPE during formation of Typhoon Ketsana in the control WRF experiment (green), sensitivity test with strengthened MCS4 (black) and weakened MCS4 (yellow).

http://dx.doi.org/10.5772/64185

Since the circulation associated with Typhoon Ketsana's formation did not move much, the area-average CAPE time series also shows the consumption and recovery cycle on the day of 1200 UTC, October 17–18 (**Figure 20**, control experiment). In order to study the MCS activities of Ketsana, Lu et al. [10] designed three sensitivity experiments on the impacts of MCSs on the early intensification rate. The same set of experiments is applied here to analyze the CAPE consumption and recovery cycles. Base on satellite images, the MCS3, MCS4, and MCS5 regions are identified as (12.8–15.8°N, 127.8–130.8°E), (15.8–18.8°N, 130.8–133.8°E), and (128–178°N, 127.8–130.8°E), respectively. In the sensitivity experiment 1, the area-averaged relative humidity in the MCS3 region between 200 and 700 hPa at 1200 UTC on October 17, 2003, which was higher than that around MCS4, is assimilated into the MCS4 region within the 6-h assimilation window (similarly for later experiments), in order to strengthen the intensity of MCS4. In experiment 2, MCS4 is weakened, and only 60% of the 200–700 hPa relative humidity in the control experiment is retained and then assimilated at 1200 UTC on October 17, 2003.

The sensitivity experiments in **Figure 20** show different CAPE consumption and recovery cycles of Typhoon Ketsana. When convection in the MCS4 is stronger (black line), the CAPE drops much more than in the control experiment during late October 17. However, the recovery of CAPE is quite efficient after, and by 0600 UTC on October 18, the average CAPE value is not much lower than that in the control experiment. The early intensification rate of Ketsana is actually faster than that of the control in this experiment. On the other hand, when convection in the MCS4 is weaker (yellow line), the average CAPE consumed is less initially, then builds up slightly, and goes through another cycle before the TC formation. Although the CAPE level near formation time in this experiment is similar to that in the control, the weakened MCSs lead to a slower formation and early intensification rate.

Similar experiment as in the second sensitivity experiment of Typhoon Ketsana was performed for Typhoon Dan (green line in **Figure 18**). With a weakened MCS, CAPE consumption before Dan's formation is much smaller than that in the control. Due to the weaker convection, the early intensification rate of the simulated typhoon is also slower. After that, CAPE recovery is still quite efficient in the environment, but has not increased to the same level as in the control experiment. Therefore, from the comparison of the two typhoon cases here, it can be concluded that the rate of TC formation directly depends on how much each convection episode associated with MCS contributes to spinning up the low-level vorticity, which has been pointed out in previous studies. On the other hand, it can also be seen that how CAPE recovers in the developing TC depends on the earlier convection episodes, but not only on the large-scale environment. The control by this factor on the pace of TC's early development deserves more case studies.

8. Discussion and conclusions

It has been observed that the time for the tropical disturbances to develop into tropical storm varies with quite a large range, and is dependent on the synoptic pattern. For example, in analyzing the MCS activities during TC formations in the WNP, Lee et al. [1] found that for

formations with a single MCS, some of them associated with easterly waves usually take an average of 13 h to form a TC. In contrast, for monsoon trough-related formations, there are usually more than two MCSs, and the average time to form a TC is about 1 day. Very often, more than one MCS coexist at the same time within the monsoon trough. Whereas recent studies on TC formations, such as Refs. [10, 21, 22], focused on contributions from convective-scale systems such as vortical hot towers (VHTs) and convectively induced vorticity anomalies (CVAs), their interactions with mesoscale circulations, and mechanisms to generate the core surface vortex, less discussion was on the relationship between convection patterns and development times of TCs. The numerical simulations of typhoons Dan and Ketsana here illustrate that the pace of early development of a TC depends much on the convection configuration, namely, whether it is a single MCS or interacting multiple MCSs.

It might seem to be counterintuitive that the multiple MCS convection pattern is not speeding up the TC development process due to spinning up of larger relative vorticity within more areas in the TC, but rather slowing the process down compared with the single MCS pattern. Nevertheless, this phenomenon may be explained from the point of view of competing for convective resources. Whenever deep convection occurs, the environmental CAPE is consumed. Descent of cold and dry air left by heavy precipitation is unfavorable for new convection development, which has to wait until the environmental CAPE increases again by heat and moisture fluxes from the ocean surface. When Ref. [21] analyzed the simulated formation of Hurricane Dolly (2008), similar processes were found under the TC system scale, namely, there were episodes of deep convection during the development of Hurricane Dolly, but in between there was a period when the CAPE was minimum. This interpretation is consistent with the simulation for Typhoon Ketsana, especially during the development of MCS3 and MCS4. These two MCSs developed at about the same time with a large area of convection, but did not lead to TC formation right after. The reason may be that MCS4 to the east was consuming part of the CAPE within the TC area, making the MCS3 to the west less conducive to developing more deep convection and subsequent low-level vorticity generation. In fact, MCS3 dissipated first, and the system intensification slowed down before another MCS developed in the core region.

It is interesting that this kind of CAPE argument is also applicable to the convective scales, as has been briefly discussed in Ref. [21]. Various convection processes, such as waxes and wanes, merging and splitting within each MCS are common during the early development of TC. That is, these processes represent the variability of the convective-scale VHT and CVA activities of the MCS, which is likely also due to the consumption and recovery cycles of CAPE. One point to note is that since the single-MCS convection pattern has been identified as the most common one at the end of early development, that is, for the TC to enter the intensification phase, the convection within that single MCS has to be long-lasting enough for the system to intensify to a sustainable level. In other words, there may be a hypothesis that the CAPE consumption and recovery cycles to sustain convection are more efficient under convective scales compared with mesoscales. This may be due to the fact that the areas for the surface fluxes to keep the low-level atmosphere warm and moist are simply much smaller, and/or that merging of the VTHs/CVAs is effective to sustain deep convection, especially when these systems are moving toward

http://dx.doi.org/10.5772/64185

the TC center under the system-scale convergent flow. However, these assertions have to be verified by further investigations.

In the case that merging of MCSs occurs, the resulted mesoscale vortex may lead to faster system intensification rather than the retardation as obtained in the earlier simulations [23–25]. More numerical studies on TC cases with explicit MCS merging have to be conducted to validate such hypothesis.

Author details

Kevin K. W. Cheung* and Guoping Zhang

*Address all correspondence to: kevin.cheung@mq.edu.au

Department of Environmental Sciences, Macquarie University, Sydney, New South Wales, Australia

References

[1] Lee, C.-S., K. K. W. Cheung, J. S. N. Hui, and R. L. Elsberry, 2008: Mesoscale features associated with tropical cyclone formations in the western North Pacific. Mon. Weather Rev., 136, 2006–2022.

[2] Laing, A., and J. Evans, 2011: Chapter 8, Introduction to Tropical Meteorology, 2nd edition, The Comet Program, U.S. University Corporation for Atmospheric Research.

[3] Zehr, R. M., 1992: Tropical Cyclogenesis in the Western North Pacific. PhD Dissertation. Colorado State University, Fort Collins, CO.

[4] Gray, W. M., 1998: The formation of tropical cyclones. Meteorol. Atmos. Phys., 67, 37–69.

[5] Vigh, J. L., and W. H. Schubert, 2009: Rapid development of the tropical cyclone warm core. J. Atmos. Sci., 66, 3335–3350.

[6] ATCR, 2003: Annual Tropical Cyclone Report, Joint Typhoon Warning Center, U. S. Naval Pacific Meteorology and Oceanography Center, 827 pp.

[7] ATCR, 1999: Annual Tropical Cyclone Report, Joint Typhoon Warning Center, U. S. Naval Pacific Meteorology and Oceanography Center, 214 pp.

[8] Riosalido, R., O. Carretero, F. Elizaga, and F. Martin, 1998: An experimental tool for mesoscale convective systems nowcasting. SAF Training Workshop on Nowcasting and Very Short Range Forecasting, 9–11 December, Vol. 25, Madrid, Spain 127–135.

[9] Fu, B., T. Li, M. S. Peng, and F. Weng, 2007: Analysis of tropical cyclogenesis in the western North Pacific for 2000 and 2001. Weather Forecast, 22, 763–780.

[10] Lu, X., K. K. W. Cheung, and Y. Duan, 2012: Numerical study on the formation of Typhoon Ketsana (2003). Part I: roles of the mesoscale convective systems. Mon. Weather Rev., 140, 100–120.

[11] Johnson, R. H., 1984: Partitioning tropical heat and moisture budgets into cumulus and mesoscale components: implications for cumulus parameterization. Mon. Weather Rev., 112, 1590–1601.

[12] Houze, R. A., 1989: Observed structure of mesoscale convective systems and implications for large-scale heating. Q. J. R. Meteorol. Soc., 115, 425–461.

[13] Steiner, M., and R. A. Houze, Jr., 1993: Three-dimensional validation at TRMM ground truth sites: some early results from Darwin, Australia. Preprints, 26th Conference on Radar Meteorology, Norman, Am. Meteorol. Soc., 417–420.

[14] Steiner, M., R. A. Houze, and S. E. Yuter, 1995: Climatological characterization of three-dimensional storm structure from operational radar and rain gauge data. J. Appl. Meteorol., 34, 1978–2007.

[15] Wang, Z., M. T. Montgomery, and T. J. Dunkerton, 2010: Genesis of pre-hurricane Felix (2007). Part II: warm core formation, precipitation evolution and predictability. J. Atmos. Sci., 67, 1730–1744.

[16] Molinari, J., S. Skubis, and D. Vollaro, 1995: External influences on hurricane intensity. Part III: potential vorticity evolution. J. Atmos. Sci., 52, 3593–3606.

[17] Molinari, J., D. Vollaro, F. Alsheimer, and H. E. Willoughby, 1998: Potential vorticity analysis of tropical cyclone intensification. J. Atmos. Sci., 55, 2632–2644.

[18] Chen, W., M. Takahashi, and H.-F. Graf, 2003: Interannual variations of stationary planetary wave activity in the northern winter troposphere and stratosphere and their relations to NAM and SST, J. Geophys. Res., 108, 4797.

[19] Chen, Y., and M. K. Yau, 2001: Spiral bands in a simulated hurricane. Part I: Vortex Rossby wave verification. J. Atmos. Sci., 58, 2128–2145.

[20] Martinez, Y., G. Brunet, M. K. Yau, and X. Wang, 2011: On the dynamics of concentric eyewall genesis: space-time empirical normal modes diagnosis, J. Atmos. Sci., 68, 457–476.

[21] Fang, J., and F. Zhang, 2011: Initial development and genesis of Hurricane Dolly (2008), J. Atmos. Sci., 67, 655–672.

[22] Zhang, D.-L., L. Tian, and M.-J. Yang, 2011: Genesis of Typhoon Nari (2001) from a mesoscale convective system, J. Geophys. Res., 116, D23104.

http://dx.doi.org/10.5772/64185

[23] Ritchie, E. A., and G. J. Holland, 1997: Scale interactions during the formation of Typhoon Irving, Mon. Weather Rev., 125, 1377–1396.

[24] Simpson, J., E. A. Ritchie, G. J. Holland, J. Halverson and S. Stewart, 1997: Mesoscale interactions in tropical cyclone genesis. Mon. Weather Rev., 125, 2643–2661.

[25] Ritchie, E. A., 2003: Chapter 12. Some aspects of midlevel vortex interaction in tropical cyclogenesis. Cloud systems, Hurricanes, and the Tropical Rainfall Measuring Mission (TRMM), W-K. Tao and R. Adler, eds. Meteorological Monographs, 29, 165–174.

IntechOpen